VPRBP functions downstream of the androgen receptor and OGT to restrict p53 activation in prostate cancer

Authors: Ninu Poulose[1,2*], Adam Polonski[3], Nicholas Forsythe[1], Gemma Gregg[1], Sarah Maguire[1], Marc Fuchs[1], Sarah Minner[3], Simon S McDade[1], Ian G. Mills[1,2]

[1]Patrick G Johnston Centre for Cancer Research, Queen's University, Belfast, UK, BT9 7AE.

[2]Nuffield Department of Surgical Sciences, John Radcliffe Hospital, University of Oxford, Oxford, United Kingdom, OX3 9DU.

[3]University Medical Center Hamburg-Eppendorf Department of Pathology, Hamburg, Germany, 20246

***Co-corresponding Author:** ninu.poulose@nds.ox.ac.uk

Running title: VPRBP regulates prostate cancer

Keywords: prostate cancer, androgen receptor, p53, glycosylation, COP9 signalosome

Abstract

Androgen receptor (AR) is a major driver of prostate cancer (PCa) initiation and progression. O-GlcNAc transferase (OGT), the enzyme that catalyses the covalent addition of UDP-N-acetylglucosamine (UDP-GlcNAc) to serine and threonine residues of proteins, is often up-regulated in PCa with its expression correlated with high Gleason score. In this study we have identified an AR and OGT co-regulated factor, VPRBP/DCAF1. We show that VPRBP is regulated by the AR at the transcript level, and by OGT at the protein level. In human tissue samples, VPRBP protein expression correlated with AR amplification, OGT overexpression and poor prognosis. VPRBP knockdown in prostate cancer cells led to a significant decrease in cell proliferation, p53 stabilization, nucleolar fragmentation and increased p53 recruitment to the chromatin. In conclusion, we have shown that VPRBP/DCAF1 promotes prostate cancer cell proliferation by restraining p53 activation under the influence of the AR and OGT.

Introduction

Prostate cancers typically progress through an androgen dependent phase to a castration resistant phase during treatment with anti-androgens, however AR mediated activation of transcription remains active throughout in majority of the cases (*1*). Hence a comprehensive understanding of AR signalling mechanisms during prostate carcinogenesis is instrumental in developing novel strategies to combat the disease. Studies have identified glycosylation as a key AR-regulated process in PCa cells (*2*). AR activation has been shown to enhance flux through hexosamine biosynthetic pathway (HBP) in PCa cell lines (*3*), which leads to increased bioavailability of UDP-N-acetylglucosamine, a substrate for O-GlcNAcylation as well as N-linked and O-linked glycosylation (*4*). O-GlcNAcylation, a highly dynamic and often transient post translational modification (PTM) is specifically increased in PCa tissues compared to adjacent non-malignant tissues (*5*). This PTM is regulated by two enzymes, OGT that catalyses the covalent addition of UDP-N-acetylglucosamine to serine and threonine residues of cytoplasmic, nuclear and mitochondrial proteins, and O-GlcNAcase (OGA) which removes the O-GlcNAc moiety (*6*). OGT is considered to be a metabolic rheostat whose expression is elevated in many cancers including PCa, with higher O-GlcNAc levels associated with poor prognosis of patients (*7*) (*8*). Maintenance of O-GlcNAc homeostasis is essential for the normal cellular physiology, the perturbance of which can contribute to altered cellular function and disease progression (*9-11*). There is a growing diverse list of proteins which undergo this PTM, including some of the key transcription factors such as c-Myc (*12*) and p53 (*13*).

A recent ChIP-seq study by Itkonen *et al* has demonstrated that the O-GlcNAc chromatin mark is rapidly lost upon inhibition of OGT activity by fast acting inhibitor OSMI2 (*14*) in PCa cells. This analysis revealed that the majority of the O-GlcNAc peaks were promoter associated with over 95% overlap with DNase-hypersensitive regions and markers of active promoters. In addition, majority of the O-GlcNAc peaks in AR positive PCa cell line LNCaP overlapped with

that of AR negative PCa cell line PC3, as well as with O-GlcNAc sites from previously reported studies suggesting a high degree of conservation between these cell lines of different origin. Motif enrichment analysis of these sites has shown a significant over-representation of ETS transcription factors (TF) and c-Myc, reinforcing the important relationship between O-GlcNAcylation and c-Myc activity. Independent AR ChIP-seq studies from our lab and many others have shown that the majority of AR binding sites are distal intergenic and motif enrichment suggest strong co-association of the AR with NF1 and Forkhead family transcription factors such as FOXA1 (*15*). Despite these differences, we know that both AR and OGT contribute to PCa progression. To better understand the interplay between OGT and AR in PCa, we performed a meta-analysis of these AR and O-GlcNAc ChIP-seq data focussing on promoter proximal sites. This analysis identified a small number of overlapping sites and genes associated with binding of AR and O-GlcNAc, and focussed on VPRBP (Vpr binding protein) also known as DCAF1 (DDB1 and CUL4 Associated Factor 1) which has been implicated as a regulator of cell cycle and cell proliferation {Guo, 2016 #14}{Han, 2020 #15}. VPRBP is the substrate recognition component of cullin 4A-ring E3 ubiquitin ligase (CRL4A) complex composed of cullin4A (CUL4A), the E3 ligase Roc1, damaged DNA binding protein 1 (DDB1), as well as separate HECT type EDD/UBR5 E3 ligase (*16*). VPRBP was initially identified as a protein targeted by HIV-1 viral protein R (Vpr) to initiate host cell response leading to cell cycle arrest at G2/M by hijacking the CUL4A E3 ubiquitin ligase machinery (*17*) (*18*). It is involved in polyubiquitination (*19*), monoubiquitination (*19*) and phosphorylation (*20*) of proteins. In this study we show that VPRBP is a novel AR target as well as an OGT regulated protein. Knockdown of VPRBP led to a marked reduction in PCa cell proliferation. We went on to show that VPRBP down-regulates p53 stability and activity, and that this is in part by maintaining nucleolar integrity. Since VPRBP is known to interact with COP9 (Constitutive photomorphogenesis 9 signalosome (CSN) subunits (*21*), we sought

to determine whether the integrity of CSN is important in maintaining VPRBP function and found that to be the case. Tissue microarray datasets showed a positive correlation of VPRBP expression with AR/OGT expression and an inverse correlation with PSA recurrence free survival. We conclude that VPRBP acts a novel downstream effector of AR and OGT mediated PCa cell proliferation by impairing p53 checkpoint activation.

Results

Identification of VPRBP as a novel AR regulated target gene

We have previously sought to gain insights into the effects of O-GlcNAcylation on transcription in PCa using ChIP-seq (*14*). To identify AR and O-GlcNAc modification co-regulated genes, we analysed published AR (GSE28126) and O-GlcNAc (GSE112667) ChIP-seq data. Comparing peak distribution between AR and O-GlcNAc binding sites from these two separate studies (Figure 1A), indicated that as previously reported the majority of O-GlcNAc binding sites are promoter proximal, whereas the majority of AR binding sites are intronic or associated with distal inter-genic regions (Figure 1A). Intersecting consensus binding sites of LNCaP AR ChIP-seq data with O-GlcNAc ChIP-seq consensus sites identified only 9 overlapping binding sites, amongst which a binding site was detected within 1000bp of *VPRBP* gene TSS (Figure 1B). VPRBP presented as the most promising target to pursue further as it was found to be highly expressed in different tumor tissues (*20*) and also known to play a pivotal role in cell growth and cell cycle entry (*25*). Moreover, depletion of VPRBP in DU145 prostate cancer cells reduced cell proliferation and number of colony forming cells (*20*). However the roles of VPRBP in mediating androgen response in prostate cancer or its regulation by OGT or O-GlcNAcylation have not been reported so far.

Next, we confirmed AR and O-GlcNAc enrichment at the VPRBP promoter region by ChIP-qPCR in LNCaP cells stimulated with 1nM R1881 for 4h and 24h following 72h of androgen

deprivation (*15*). We confirmed that as expected androgen stimulation resulted in AR enrichment at a CAMKK2 associated site (a known AR target (*15*)), at both time points. O-GlcNAc enrichment identified on the previously described c-MYC site in the promoter of the PPAT/PAICS {Barfeld, 2015 #47} gene was unaltered in response to androgen treatment (Figures 1C and S1A). Androgen stimulation resulted in increased binding of AR at the VPRBP promoter region only at 24h time point coincident with a decrease in the O-GlcNAc signal (Figure 1C and S1A). Results showing relative fold enrichment with AR and O-GlcNAc ChIP at 24h time point are provided in the supplementary figure S1A.

Androgen stimulation enhances VPRBP expression in LNCaP cells

In order to determine whether an increase in AR binding to VPRBP promoter reflects an increase in the rate of transcription and protein synthesis, we looked at the expression levels of VPRBP following androgen stimulation. Quantitative RT-PCR(qRT-PCR) analysis revealed that R1881 stimulated binding of AR to VPRBP promoter correlated with a 2.5 fold increase in the expression of VPRBP mRNA at 24 h (Figure 1D), concomitant with significant increase of VPRBP protein levels 24 and 48 hours (Figures 1E and S1B). OGT and O-GlcNAcylation levels (detected by RL2 antibody) also showed significant increases following R1881 stimulation at the later time points (Figure 1E). CAMKK2 and UAP1 expression levels were used as positive controls (*15*) which showed significant increases in protein expression with 12h time point onwards. Since R1881 is a synthetic androgen, we also tested the effect of endogenous androgen, dihydrotesteosterone (DHT). Similar to R1881, stimulation of LNCaP cells by DHT for 24h also increased VPRBP mRNA and protein expression (Figures S1C and S1D).

We also observed a reduction in p53 protein (Figure S2A) and mRNA expression (Figure S2B) in LNCaP cells following R1881 stimulation, and a corresponding decrease in p53 enrichment

at p21 (CDKN1A) promoter by ChIP-qPCR (Figure S2C) suggesting that pro-proliferative effects of androgens may partly be mediated by factors that downregulate p53. However VPRBP itself does not appear to be p53 regulated, since there was no significant enrichment by ChIP-qPCR (Figure S2D) and no binding sites were identified within its promoter region from p53 ChIP-seq in nutlin-3a treated LNCaP cells (Figure S2E). Analysis of a novel CRISPR p53 knockout LNCaP cell-line showed enhanced levels of VPRBP; by contrast treating LNCaP cells with a p53 stabilizer, nutlin-3a, led to decrease in VPRBP (Figures S2F and S2G). Consequently a reciprocal feedback relationship between VPRBP and p53 expression seems to exist within these cells.

OGT is required for VPRBP stability.

To determine if OGT is required for VPRBP expression, we performed OGT siRNA knockdown. This revealed that there was no significant change in basal VPRBP mRNA levels in OGT siRNA transfected cells compared to scrambled control (Figure 2A). Interestingly, basal (Figure 2B) as well as R1881 induced (Figure 2C) VPRBP expression was reduced at the protein level in OGT siRNA transfected cells compared to scrambled control. OGT siRNA transfection resulted in >90% reduction in basal OGT protein expression and >80% reduction in total O-GlcNAc levels with both siRNAs (Figure S3A). There was ~57% reduction in VPRBP protein expression with OGTsiRNA1 and ~54% with OGT siRNA2 5d post transfection (Figure S3A). A significant reduction in p53 protein expression was observed with OGT siRNA2 (~30%) but not OGTsiRNA1 (~13%) ((Figure 2B and S3A). Overall, these results suggest a possible dual regulation of VPRBP, whereby VPRBP is induced at the mRNA level by AR and is stabilised post-translationally by OGT activity. This also explains the higher fold increase in VPRBP protein level with androgen treatment at 24 h compared to transcript level, owing to both androgen dependent increase in transcription as well as OGT mediated stabilization of translated protein.

O-GlcNAcylation has been shown to affect the stability of proteins like p53 (*13*), c-Myc (*3*) and EZH2 (*26*). Therefore we performed immunoprecipitation (IP) studies to test the O-GlcNAcylation status of VPRBP. IP indicates that VPRBP is an O-GlcNAcylated protein (Figure 2D). To further confirm if O-GlcNAcylation is necessary for the stability of VPRBP, we treated the cells with fast acting inhibitors of OGT activity, OSMI2 and OSMI3 (*27*). It was found that treatment for 24h decreased VPRBP expression at the protein level by ~73% for 40 μM OSMI2 and ~62% for 10 μM OSMI3 (Figure 2E). OSMI treatment reduced overall O-GlcNAcylation levels with a compensatory upregulation of OGT expression (Figures 2E and S3B). There was no significant change in VPRBP expression at the transcript level with OSMI3 treatment, although OSMI2 exhibited a small reduction of VPRBP transcripts (Figure S3C). These studies do not preclude the possibility of VPRBP stabilization through interaction with other O-GlcNAcylated protein/s.

VPRBP down-regulation stabilizes p53 and inhibits LNCaP cell proliferation

Having identified VPRBP as an AR-regulated gene as well as an O-GlcNAc regulated protein, we went on to determine the functional effect of VPRBP knockdown in LNCaP. Knockdown with VPRBP siRNA resulted in ~75% reduction in VPRBP mRNA expression 3d post transfection (Figure 3A). A ~57% reduction in cell number was observed with VPRBP siRNAs when cells were grown in complete growth media containing androgens whereas androgen deprivation on its own resulted ~38% in a reduction in cell numbers as assessed by cell counting 5d post transfection (Figure 3B). Furthermore, chemical inhibition by B32B3, a potent and selective inhibitor of VPRBP kinase activity (*20*), led to ~64% decrease in LNCaP cell proliferation at 5μM concentration (Figure S4A). B32B2 5μM also decreased histone H2A threonine 120 phosphorylation as previously shown by Kim *et al (20)* in DU145 cells though we did not observe significant changes with lower doses (S4B). The combination of B32B3 and OGT inhibitors did not show significant decreases in cell numbers (Figure S4A).

Since VPRBP deletion in T lymphocytes was previously shown to cause drastic stabilization of p53 (*25*), we looked at the p53 status following VPRBP knockdown in LNCaP. VPRBP knockdown in LNCaP led to a substantial increase in p53 expression and its downstream targets p21 and Mdm2 (Mouse double minute 2 homolog), (Figures 3C and Fig S4C). Although Mdm2 is a negative regulator of p53 at the protein level, Mdm2-p53 relation is rather complex with stabilized p53 transcriptionally activating Mdm2 gene (*29*). Cyclin dependent kinase inhibitor, p21 is well known for its role in induction of G1 arrest (*28*). Consequently we observed a drastic reduction in cell cycle markers like phospho CDK2 Thr160 (*31*) (which activates CDK2 complexes and a marker of G1/S), Cyclin B1 (*32*) (a marker of G2/M phase), polo-like kinase1 (PLK1) (*33*)(a marker of late G2 that promotes mitotic entry), phospho-histone H3 ser10 (*34*) (marker of mitotic chromatin condensation) and Phospho-PP1α Thr320 (*35*) (Figures 3C and Fig S4C) following VPRBP knockdown. There was also a significant decrease (~35%) in the expression of proto-oncogene cMyc with VPRBP siRNA2. In summary, VPRBP tightly control cell proliferation mainly by regulating the expression of p53.

It is interesting to note that whereas VPRBP knockdown led to p53 stabilization, the reduction in VPRBP levels by OGT knockdown did not translate to similar effects (Fig. 2B). This is likely because p53 itself is an O-GlcNAcylated protein whose stability is enhanced with O-GlcNAcylation at Ser 149 position (*13*). Therefore a decrease in p53 O-GlcNAcylation/stabilization by OGT knockdown likely negates its stabilization with VPRBP reduction. This may be one of the reasons why OGT knockdown (~23% reduction) (Figure S4D) had a lesser effect on LNCaP proliferation compared to VPRBP knockdown (Fig 3B). This also implies a combination of OGT inhibitor with VPRBP inhibitor or inhibitors which can stabilize p53 like nutlin 3A would be better agents in regulating prostate cancer growth.

We next wanted to determine if the growth inhibitory effects of VPRBP knockdown were primarily mediated through p53 stabilization and activation. For this, we resorted to VPRBP

knockdown in VCaPs, a cell line that express a p53 heterozygous mutant. In VCaPs, VPRBP knockdown failed to cause significant changes in cell numbers (Figure 3D) and cell cycle markers (Figure 3E), indicating a crucial role for p53 in mediating VPRBP effects in PCa. Similar to LNCaP, VPRBP knockdown in VCaP cells also showed a reduction in c-Myc (Figure 3E). Together, these results suggest that the growth inhibitory effects of VPRBP knockdown were mainly mediated through p53 stabilization and activation.

p53 ChIP-seq reveals increased p53 recruitment to the chromatin following VPRBP knockdown

To further corroborate the above findings, we performed p53 ChIP-seq in LNCaP cells following siRNA knockdown with VPRBP, OGT and non-targeting siRNAs along with nutlin-3a treated samples. Canonical p53 target gene p21 (CDKN1A) was used as a positive control to validate ChIP efficiency by ChIP-qPCR (Figure 4A). This is the first report on p53 ChIP-seq in a prostate cancer cell line. Overall, p53 ChIP-seq in LNCaP gave lesser number of peaks (Figure 4B) compared to previously reported studies in other cell types (*36, 37*), suggesting fundamental differences in p53 transcriptional program between these cells. P53 ChIP-seq in Nutlin-3a treated LNCaP cells showed 582 peaks, the majority of which (>80%) overlapped with nutlin-3a p53 ChIP-seq binding sites in other cell lines confirming they are bona fide p53 binding sites (Figures 4C, S5A and S5B). As expected from our data, we observed a ~4.7 fold increase in the number of p53 genomic binding sites following VPRBP knockdown compared to scrambled si or OGT knockdown (Figure 4B). Whereas VPRBP si1 p53 ChIP-seq showed 2326 binding sites, VPRBP si2 had 1639 binding sites. ~85% of VPRBP si2 peaks (1387) overlapped with that of VPRBP si1 peaks (Figure S5C). 90% of LNCaP nutlin-3a p53 ChIP-seq sites overlapped with VPRBP si consensus sites (Figure 4D). Majority of VPRBP si consensus peaks overlapped with nutlin-3a MCF7 p53 ChIP-seq peaks (Figure 4E). Though there were some differences in the peak distribution among OGT si1 and OGT si2, majority of

the sites overlapped (Figure S5C). There was also a significant overlap of OGT si consensus sites with VPRBP si consensus sites and scr si sites (Figure S5C).

The majority of chromatin-bound p53 was found in distal intergenic regions (45-54%), with around 4.5-6% binding events with in 3000bp of TSS, under the different conditions tested (Figure S5D). This resembled the AR binding pattern, which is mostly intronic or associated with distal inter-genic regions, as opposed to O-GlcNAc binding sites which are mostly promoter proximal (Figure 1A). The p53 ChIP-seq peaks in other cell lines also followed more or less similar binding profiles suggesting conservation of p53 binding across different cell types (Figure S5D). The sites enriched in VPRBP knockdown compared to scrambled were obtained, and the genes associated with these sites were generated using BETA-minus tool in galaxy cistrome (Supplementary file 2). Motif enrichment analysis showed an over-representation of TP53, TP73 and TP63 binding motifs (Figure S5E).

VPRBP knockdown induces nucleolar stress in LNCaP cells

Previous studies have underscored the importance of OGT and O-GlcNAcylation in regulating translation and ribosome biogenesis (*38*). Interestingly, VPRBP has also been shown to be a factor involved in 40s ribosomal subunit biogenesis in human cells along with other CRL4 E3 ubiquitin ligase and COP9 signalosome components in a genome wide RNAi screen study (*39*). Ribosome biogenesis occurs within the nucleoli, which also acts as stress sensor in mammalian cells by regulating Mdm2 association with p53, subsequent ubiquitination and degradation of p53 (*40*). Nucleolar stress is known to induce p53 stabilization and cell cycle arrest by disrupting Mdm2-p53 interaction. A recent study by Han *et al* revealed a critical role for VPRBP in rRNA processing and ribosome biogenesis by regulating a previously unknown substrate, the ribosome assembly factor PWP1 {Han, 2020 #15}. Interestingly, VPRBP loss

leads to accumulation of free ribosomal protein L11 (RPL11), resulting in L11-MDM2 association and p53 activation.

VPRBP has been previously shown to localize in the cytoplasm (*17*) as well as nucleus (*41*). A comparison of VPRBP interactome (147 proteins) obtained from BioGRID database (*42*) (supplementary file 3) with nucleolar proteome (1314 proteins) of human cells derived from the Cell Atlas (*43*) showed that ~14 % of VPRBP interactors also show nucleolar localization (Figure 4F). Hence we hypothesised that VPRBP knockdown may enhance p53 stability and diminish ribosome biogenesis by destabilising the nucleolus. Our iimmunofluorescence studies showed both cytoplasmic and nucleolar localization of VPRBP (Figure 4G). Reduction in the number of nucleoli and/or disintegration of nucleolar structures are some of the characteristic features of nucleolar stress (*44*). We found a marked change in staining pattern of nucleolar protein fibrillarin following VPRBP siRNA knockdown, indicative of nucleolar stress (Figure 4G). Fibrillarin showed exclusive nucleolar localization with a redistribution to small nucleoplasmic entities in the VPRBP knockdown cells, similar to previously described with actinomycin D treatment (*45*). A significant (~25%) reduction in fibrillarin and 40S ribosomal protein S8 (RPS8) expression, was observed with VPRBP siRNA2 (Figures S6A and S6B.) P53 stabilization is a complex process involving a series of posttranslational modifications and interactions with other proteins. A further characterization of role of VPRBP in maintaining nucleolar integrity would be important to uncover the underlying mechanism.

COP9 signalosome is a key regulator of VPRBP stability and p53 regulation.

COP9 signalosome (CSN) is an essential regulator ubiquitin-proteasome-dependent degradation of many tumor suppressors and oncoproteins by deneddylation and inactivation of the cullin subunit of Cullin-RING ubiquitin ligases (CRL) (*46*). It's also known that phosphorylation of p53 at Thr 155 by CSN targets p53 to ubiquitin–26S proteasome-dependent

degradation (*47*). VPRBP has been reported to be present in a mega complex comprising subunits of CRL4 complex and CSN in T cells (*25*). Many of the CSN subunits were found to be VPRBP interacting proteins from Biogrid database including COPS3, COPS4, COPS5, COPS6, COP7A, COPS7B and COPS8 (Supplementary file 3). COPS2, COPS3, COPS4, COPS5 and COPS8 were also found to be indispensable for 40s ribosome subunit biogenesis. Therefore we sought to determine the role of CSN in LNCaP cells. We found a ~1.8 fold increase in COPS3 mRNA levels with androgen stimulation for 24h (Figure 5A) which is in agreement with the gene expression data of Massie *et al* (*15*) and ~1.8 fold increase in protein levels (Figure 5B and 5C). siRNA mediated downregulation of COPS3 resulted in 87% and 80% reduction in COPS3 mRNA with siRNAs 1 and 2 respectively (Figure 5D). COPS3 downregulation led to a remarkable reduction in VPRBP proteins levels (Figure 5E) without reduction in mRNA levels (Figure 5D). COPS3 knockdown also affected the stability of other CSN components like COPS2 and COPS5. COPS3 knockdown also led to stabilization of p53 and its target p21 5d post transfection (Figure 5E). COPS3 expression, however did not change with VPRBP knockdown (Figure 3C). There was ~27% reduction in cell numbers observed at 5d post transfection (Figure 5F). These results suggest that integrity of CSN is a key factor in maintaining VPRBP stability and that the CSN effect on p53 is likely mediated through VPRBP.

Since CSN catalyzes CRL deneddylation, we tested the effect of a selective NEDD8 activating enzyme inhibitor, MLN4924 on LNCaP proliferation. MLN4924 was found to inhibit LNCaP cell proliferation in a dose-dependent manner (Figure 5G). Interestingly, the combination of MLN4924 and OGT inhibitors was found to be more effective in these cells (Figure 5H).

VPRBP expression correlates with AR expression in clinical samples and is prognostic

Having identified as a novel AR targeted gene, we wanted to determine the clinical relevance of this protein in PCa. A previous study by Kim *et al* reported high expression of this protein in DU145 prostate and MDA-MB231 breast cancer cell lines (*20*). This study also reported VPRBP overexpression in multiple cancer tissues including breast and prostate tumour samples compared to their benign counterparts by IHC. To further understand the prognostic potential of VPRBP in PCa, we analysed its expression in tissue microarrays by IHC and its correlation with tumor phenotype, and protein markers including the AR and OGT. Nearly 50% of all tumours stained strongly for VPRBP irrespective of the tumor stage. There was also a marked reduction in percentage of VPRBP negative tumors with higher tumor stage (Supplementary table 6). However, there were no drastic changes in VPRBP expression between patients with no regional lymph node metastasis (N0) and patients with metastasis (N+). Comparison of quantitative Gleason Grade suggested an overall increase in VPRBP staining with increased tumor Grade. Significant correlations were not seen in VPRBP expression with preoperative PSA levels. A higher VPRBP staining was observed in cases with positive surgical margins. VPRBP expression strongly correlated with AR expression which was expected to be the case from our *in vitro* studies (Figure 6A). Likewise, VPRBP expression positively correlated with OGT expression (Figure 6B). The representative images of negative, low, intermediate and high staining of VPRBP are shown in Figure S6C. Finally, an inverse correlation between VPRBP expression and PSA recurrence free survival was observed (Figure S6C). By scoring stratifying the cases according to either a combination of VPRBP and AR scoring or VPRBP and OGT scoring we were able to stratify the patients into more significant poor prognosis groups. These were defined in both cases by high expression of the two proteins (Figure 6C and 6D).

Next we compared the VPRBP mRNA expression in TCGA PanCancer Atlas datasets and found a positive correlation with AR mRNA expression and inverse correlation with

HALLMARK_P53_pathway (genes involved in p53 pathways and networks) (Figures 6D and 6E). Together these studies underscore the significance of VPRBP in promoting PCa growth and progression.

Discussion

O-GlcNAcylation biology has gained a considerable interest in the recent years with remarkable advances in our understanding of its spatial and temporal functions, and targeted proteins (*12*). OGT plays a central role in setting the transcriptional landscape of the cells, proto oncgene c-Myc being one of its prime targets (*48*) whose overexpression in PCa is associated with biochemical recurrence(*49*). Our previous studies attributed the impact of O-GlcNAc/OGT on PCa cells to effects on c-Myc stability (*3*), and based on ChIP-seq data, to the over-representation of c-Myc at O-GlcNAc binding sites in the genome (*14*). Collectively this implied that a significant proportion of O-GlcNAc-labelled chromatin contained c-Myc transcriptional complexes owing to OGT dependent stabilization of c-Myc. Though the majority of O-GlcNAc peaks in the genome are promoter proximal and associated with histone marks indicative of active transcription (*14*), the majority of AR sites are distal intergenic. Genome-wide motif co-enrichment, have shown entirely distinct associations between O-GlcNAc and other factors (principally c-Myc and ETS transcription factors), and the AR and other factors (Forkhead family transcription factors such as FOXA1)(*15*). However, we observed that a small number of AR binding sites overlapped with O-GlcNAc sites on chromatin and hypothesised that these might help us to identify factors that were co-regulated by the AR and OGT. The potential biological significance of these sites is underscored by the fact that in our case they have led us to focus on VPRBP which is known to have significant and wide ranging effects on cell cycle and proliferation.

VPRBP was initially discovered as a target of HIV1 viral protein vpr employed to usurp the host ubiquitin machinery and induce cell cycle arrest in the G2 phase (*18*). This implies that VPRBP can in some settings support cell cycle progression and indeed we know this to be the case from previous studies (*50*). On the other hand, in T cells it regulates activation induced T-cell growth and cell cycle entry (*25*). Intriguingly OGT is also known to be required to sustain T cell proliferation and clonal expansion by stabilising c-Myc (*51*). This provides a precedent for believing that VPRBP may be of fundamental importance to the OGT- and AR-dependent proliferation of PCa cells. We show that VPRBP is transcribed in response to androgen treatment (Figure 1E) and that its protein stability is dependent on OGT (Figures 2B, 2C & 2E). We went on to show that knockdown of VPRBP by siRNA led to significant decrease in LNCaP proliferation accompanied by stabilization of tumor suppressor p53 (Figure 3C). Guo *et al* (*25*) demonstrated similar stabilization of p53 in T cells following VPRBP deletion suggesting its requirement in Mdm2-mediated p53 poly-ubiquitination (*25*). They further show that VPRBP requirement for cell cycle entry is independent of cell growth which precedes cell cycle entry in naive T cells after T-cell receptor (TCR) activation (*25*). For T cell proliferation to occur, VPRBP promotes cell cycle entry by restraining p53 activation whilst a VPRBP-dependent, p53-independent programme possibly involving c-Myc dictates cell growth. They went on to show that VPRBP is essential for T-cell-mediated anti-viral and autoimmune response. One can draw some similarities between T cells progressing from quiescence to proliferation and cancer cells during malignant transformation. During TCR, cells undergo dramatic metabolic changes with increased glucose and glutamine uptake, and a concomitant increase in O-GlcNAcylation (*52*). Comparably, androgen stimulation of PCa cells increased glucose uptake and anabolic synthesis of glutamine (*15*). Androgen stimulated cells also displayed higher HBP pathway enzymes and protein O-GlcNAcylation levels. Interestingly, VPRBP is upregulated on TCR activation as well as with AR activation in PCa cells which

indicates a similar underlying biology between these two cell types. Collectively our data suggest that the similar dependencies on both VPRBP and OGT for cell proliferation exist for both PCa cells and T cells, particularly in cancer cases that are p53 wild-type.

Other than stabilization, the regulation of p53 transcriptional activity by VPRBP has been previously described by Kim *et al* (*53*) to occur at the chromatin level. In this study they showed that VPRBP is recruited to target promoters by p53 to attenuate p53 dependent transcription by selectively binding to the unacetylated histone H3 tails in the absence of any stress stimuli rendering it inaccessible to Histone acetyl transferases. They also showed that VPRBP knockdown led to activation of p53 target genes, so did its phosphorylation at ser-895 by DNA-activated protein kinase (DNA-PK). A follow up study by the same group further identified a novel intrinsic kinase activity of this protein towards histone H2A on threonine 120 which favours its localization to tumor suppressor genes and chromatin silencing (*20*). In our study we have shown that VPRBP knockdown significantly enhances the recruitment of p53 to chromatin as assessed by a significant increase in genome-wide p53 binding sites. Furthermore so this impact may indeed be due to the reported kinase activity of VPRBP since LNCaP cells were sensitive to the VPRBP kinase inhibitor, B32B3. VPRBP can also impact chromatin through TET family of enzymes so does OGT. Monoubiquitylation of TET proteins by VPRBP promote their binding to chromatin to regulate gene by iterative oxidation of 5-methylcytosine to 5-carboxy cytosine (*19*). Interestingly independent studies also show physical and functional interaction of OGT with TET proteins, predominantly at transcription start sites that contain CpG islands (*54*). These studies highlight a putative interdependency of OGT and VPRBP in regulating gene transcription. Collectively, these suggest that VPRBP is a multi-stage inhibitor of p53 activation, impacting on both chromatin binding and p53 stability and expression. This impact may however be most profound in cells expressing wild-type p53 since a mutant p53 cell-line, VCaP, did not show significant reductions in p53 levels with VPRBP knockdown.

We also tested the feedback effects of p53 activation on VPRBP expression and have found that stabilising p53 pharmacologically with nutlin-3a diminishes VPRBP stability and knocking out p53 enhances it (Figure S2F). We believe this is predominantly a post-translational/protein turnover effect since there are no significant changes in transcript levels and no evidence of p53 binding to the VPRBP promoter (Figure S2G) and it is also known that VPRBP can form a complex with Mdm2 and p53 (*25*). All the above studies suggest a reciprocal relation between p53 and VPRBP dependent on the balance between OGT and AR activity in prostate cancer cells. Since VPRBP effects are mostly mediated through p53, targeting VPRBP would be effective in a subset of PCa without p53 mutations. Whereas one hand p53 is negatively regulated by VPRBP, on the other hand it's stabilized by OGT which explains an absence of p53 stabilization with OGT knockdown despite of decreased VPRBP levels.

In previous studies we have identified c-Myc genes and pathways in PCa that impact p53 stability. An important example was IMPDH2 which is involved in the de novo purine nucleotide biosynthesis pathway. In that study we reported that inhibiting this enzyme with a drug, mycophenolic acid, led to p53 stabilisation by depleting cellular GTP levels, promoting degradation of nucleolar proteins such as GNL3 and thereby inducing nucleolar stress (*55*). Interestingly mycophenolic acid was developed and used initially to restrict T and B cell proliferation for the purposes of enhancing graft take in patients undergoing renal transplant surgery (*56*). This further reinforces the idea that there are significant commonalities in the biological processes that support immune activation mediated T-cell proliferation and PCa cell proliferation. Additionally this study also further highlighted the established importance of the nucleolus as a nuclear sub-compartment critical to the stability of the Mdm2-p53 complex as well as to supporting ribosome biogenesis and Myc activity. Since we had observed this close feedback relationship between c-Myc and p53 centred on nucleolar integrity and function, we

were led to test how targeting VPRBP might affect this compartment. Around 14% of VPRBP interactome showed nucleolar localization suggesting its potential role in maintaining nucleolar integrity. Imaging of nucleolar marker, fibrillarin revealed marked changes in nucleolar staining indicative of nucleolar stress (Figure 4G). Together, we conclude that VPRBP restricts p53 activation in part by maintaining nucleolar integrity.

VPRBP was found to be a weakly O-GlcNAcylated protein from our IP study. It is known that O-GlcNAcylation plays important roles in regulating translation and ribosome biogenesis with many of the core ribosomal proteins being O-GlcNAc modified (*38*). VPRBP along with subunits of COP9 signalosome complex have previously shown to sustain 40S ribosome subunit biogenesis by supporting nucleolar integrity (*39*). CSN regulates the activity of CRLs, the largest family of E3 ubiquitin ligases by deneddylation (*57*). In the present study, we observed an androgen dependent increase in COPS3 expression at transcript and protein levels (Figures 5A and 5B). In addition, COPS3 knockdown led to VPRBP down-regulation and p53 stabilization (Figure 5E). While in normal cellular conditions, p53 undergoes rapid degradation by ubiquitin dependent proteolysis, cellular stress results in p53 stabilization. P53 stabilization occurs mostly at the post-translational level, mainly by phosphorylation. Phosphorylations at Ser 15, Thr 18 or Ser 20 in the in Mdm2 binding region reduce its interaction with Mdm2 which is required for its degradation by ubiquitin−proteasome pathway (*58*). On the contrary phosphorylation at Thr 155 by CSN associated kinases promotes its degradation by the ubiquitin–proteasome pathway (*47*). Interestingly, a recent study has shown that VPRBP loss leads to accumulation of free ribosomal protein L11 (RPL11), resulting in L11-MDM2 association and p53 activation {Han, 2020 #15}. Other mechanisms of p53 stabilization include acetylation and sumoylation. It is to be noted that whereas VPRBP knockdown does not affect COPS3 protein levels, COPS3 knockdown markedly reduced VPRBP expression. In T cells also stability of CSN components seems to be unaffected by VPRBP knockdown (*25*). The

mechanism through which CSN regulates VPRBP stability would need to be investigated further to gain a better understanding of OGT-COPS3-VPRBP axis. CSN downregulation may be trapping CRL in neddylated state which can inactivate a subset of CRLs by inducing degradation of their substrate recognition module. CSN and VPRBP may be working in tandem to maintain p53 at low levels to favour cell growth and proliferation. It also implies that the effect of OGT on VPRBP protein levels may be partly mediated through COPS3/CSN. Though all CSN subunits are essential for the stability of the complex, deneddylation is catalysed by CSN5 subunit which has metalloprotease activity. CSN is implicated in cancer with CSN6 or CSN5 overexpression identified from analysing human cancer patient transcriptomic data sets (*59*). These studies also point towards a potential therapeutic vulnerability since inhibitors of neddylation (*60*) and also of COP9 signalosome subunit activity (*61*) are under pre-clinical and clinical development for the treatment of a number of cancer types (*62-65*). Using MLN4924 we observed a dose dependent decrease in LNCaP proliferation which was enhanced with OGT inhibition.

By examining the VPRBP protein expression in tissue from a highly annotated prostate cancer patient cohort we established that expression increases significantly with stage and grade and furthermore correlates positively with high expression of the AR and OGT. As inhibitors of the COP9 signalosome and neddylation progress through clinical trials it will be of interest to determine whether the VPRBP expression status in patient samples and the p53 status of those patients together helps to predict responses to these drugs. Future studies will also need to further dissect the functional impact of VPRBP in a range of other mutational backgrounds include RB-loss, PTEN-loss and p53 point mutation. In conclusion VPRBP represents the first AR and OGT co-regulated protein to promote prostate cancer cell proliferation by limiting p53 activation and as such may be an early determinant of prostate cancer progression. Based on our studies and previous studies on T cell proliferation and activation we believe that it works

hand-in-glove with c-Myc to support proliferation. It would be relevant to include VPRBP in patient stratification for treatment optimization in men with PCa. Further characterization of AR-OGT-VPRBP axis will have significant impact on our understanding of AR dependent prostate cancer and in developing new avenues for PCa treatment.

Materials and Methods

Reagents and consumables

Synthetic androgen, R1881 and dihydrotestosterone were obtained from Sigma-Aldrich. OGT inhibitors, OSMI2 and OSMI3 were kindly provided by Professor Suzanne Walker (Harvard Medical School, Boston, MA, USA). Formaldehyde 16% (F017/3) was purchased from TAAB laboratory. iDeal ChIP-seq Kit for Transcription Factors (C01010170) was obtained from Diagenode. Pevonedistat or MLN4924 (S7109) was purchased from Selleck Chemicals. B32B3 (SML1419) and the primary antibodies against CAMKK2, UAP1, OGA, and COPS3 were purchased from Sigma-Aldrich. The primary antibodies against AR, VPRBP, OGT, RL2, c-Myc, β-actin, Histone H2A phospho T120, fibrillarin, CSN2, JAB1/CSN5, RPS8 and RPL5 were procured from Abcam. The primary antibody against p53 was procured from Santa Cruz Biotechnology. Cyclin B1, PLK1, phospho-PP1α, phospho-Histone H3 (Ser10), phospho-CDK2, p21 antibody, HRP conjugated goat anti-rabbit and goat anti-mouse secondary antibodies were from Cell Signalling Technology. Mdm2 antibody was obtained from EMD Millipore. Antibody details are provided in supplementary table 1. Lipofectamine RNAiMAX Transfection Reagent (13778075) was obtained from ThermoFisher scientific. Protein A sepharose beads (ab193256) and protein G sepharose beads (ab193259) were from abcam. Immobilon crescendo western HRP substrate was from Millipore (WBLUR0500) and western lightning Ultra from PerkinElmer (NEL112001EA).

Cell lines

LNCaP cells were purchased from ATCC and cultured in Roswell Park Memorial Institute media (RPMI) containing 10% fetal bovine serum and 1% pencillin-streptomycin in a humidified incubator at 37^0C and 5% CO_2. VCaP cells were obtained from ATCC and cultured in Dulbecco's Modified Eagle Media (DMEM) containing 10% fetal bovine serum and 1% pencillin-streptomycin in a humidified incubator at 37^0C and 5% CO_2. TP53 CRISPR knockout LNCaP cells were provided by Dr.Simon McDade (Queen's University, Belfast, UK; supplementary methods)

ChIP-qPCR

LNCaP cells were cultured in androgen deprivation media for 3 days prior to treatment with R1881 1nM, for 24h. Cells were fixed with 1% formaldehyde and chromatin prepared by sonication in Bioruptor® Plus sonication device (Diagenode). Fragmentation efficiency was analysed using fragment analyser (Agilent Technologies) and chromatin immunoprecipitation (ChIP) carried out using diagenode iDeal ChIP-seq kit for transcription factors (C01010055). Commercially available antibodies targeted against AR, O-GlcNAc modification (RL2) and p53 were used for the IPs. Percentage recovery of immunoprecipitated DNA relative to input was calculated from real time quantitative PCR (ChIP-qPCR) Ct values. ChIP-qPCR primers were obtained from Eurofins genomics and sequences listed in supplementary table 2.

p53 ChIP-seq

For the p53 ChIP –seq studies, LNCaP cells were grown in 10 cm dishes and treated with DMSO or 2.5 μM nutlin-3a for 24h. Another set was transfected with scrambled, VPRBP or OGT siRNAs. Cells were processed as described in the previous section. ChIP-qPCR of p21 was conducted to measure the enrichment of immunoprecipitated DNA. Libraries were prepared using diagenode Microplex library preparation kit V2, pooled and sequenced using Illumina NextSeq™ 500 high output, yielding ~50 million reads per sample (NextSeq run

metrics table and Multi QC report provided in supplementary file 1). Fastq files were generated with Illumina pipeline software (bcl2fastq version 2.19 using the default thresholds). Reads were mapped to the GRCh37/hg19 reference genome using bowtie2 (version 2.2.6) and subsequently filtered to remove PCR duplicates. Prior to peak calling, Encode curated blacklisted genomic regions were removed from bam files. Fastq files were aligned to hg19 using bowtie2 (*22*). The MACS algorithm (version 2.1.2) (*23*) was used to analyse the resulting alignments and identify transcription factor binding regions. The p53 ChIP-seq data has been deposited in the NCBI GEO data repository.

ChIP-seq data analysis

Galaxy cistrome (http://cistrome.org/ap/root) and galaxy Europe (https://usegalaxy.eu/) analysis platforms were used to compare AR, O-GlcNAc and p53 ChIP-seq binding sites. For AR ChIP-seq data (GSE28126), binding sites were converted from hg18 to hg19 using the liftover tool in Galaxy cistrome. Galaxy intersection tool was used to intersect intervals of two datasets to return overlapping pieces of intervals for at least 1bp. Galaxy subtract tool was used to subtract intervals of two datasets. CEAS tool in galaxy cistrome was used to annotate ChIP binding sites and BETA-minus for target prediction. Pscan-ChIP was used for motif enrichment analysis {Zambelli, 2013 #61}. Venn diagrams were generated either in galaxy cistrome or by Venny 2.1.0.

Real time qPCR

The cells were lysed in qiazol and RNA isolated using Qiagen miRNeasy mini kit (Cat # 217004). Transcriptor first strand cDNA synthesis kit (Cat # 04897030001, Roche Life science) was used for cDNA preparation. SYBR Green 1 Master (Cat# 4887352001, Roche Life science) was used to compare gene expression changes in VPRBP, OGT, CAMKK2, UAP1, COPS3, p53 and p21 by realtime qPCR in Roche LightCycler® 480 Instrument II.

Human large ribosomal protein (RPLPO) was used as the internal control. Primers for realtime PCR were purchased from either Sigma (KiCqStart predesigned) or from Eurofins genomics. The primer details are provided in supplementary table 3 and 4 respectively.

siRNA transfection

LNCaP cells were seeded on to 6 well plates for siRNA knockdown. Forward transfection was performed the following day using Lipofectamine RNAiMAX Transfection Reagent in OPTI-MEM with 30 pmol of siRNA/well according to the manufacturer's instructions. After overnight incubation, media was changed to RPMI with 10% FBS and antibiotics. Two individual siRNAs were used against each target of interest. The siRNAs used were OGT si1, OGT si2, DCAF1 si1, DCAF1 si2, COPS3 si1, and Silencer™ Select Negative Control No.1 siRNA (Details are provided in supplementary table 5). For studies involving androgen treatment, media was changed to androgen deprived charcoal-treated media for 3 days prior to stimulation with 1 nM R1881 for 24h. The cells were lysed after given number of days post transfection for analysis by western blot or real time PCR.

Western blot analysis.

The cells were lysed in RIPA buffer (Sigma) containing protease inhibitor cocktail (Roche) and PhosSTOP^{TM} (Sigma); protein concentration estimated with Bradford reagent (Biorad) and 30 µg of lysate subjected to electrophoresis using precast 4–12% NuPage mini-gels (Life Technologies). The resolved proteins were then transferred to PVDF membrane, blocked with 5% nonfat dry milk and probed with respective primary antibodies overnight at 4^0C. After 3 washes, the blots were probed with HRP-conjugated secondary antibodies and immunoreactivity detected by enhanced chemiluminescence in Syngene G box.

Immunoprecipitation

Briefly, LNCaP cells were lysed in IP lysis buffer (10mM Tris-Cl pH7.5, 140mM NaCl, 1mM EDTA, 1% Triton X-100, 0.1% sodium deoxycholate, 0.1% SDS). Lysates were precleared with protein A sepharose beads for 1h at 4^0C in a rotator. Immunoprecipitation (IP) was carried out with protein A sepharose beads using 1mg lysate and 1 µg VPRBP antibody. Lysate was incubated with VPRBP or IgG negative control antibody for 3h at 4^0C in a rotator followed by overnight incubation with 40µl of washed protein A sepharose beads. The beads were briefly pelleted and washed thrice in IP wash buffer (10mM Tris-Cl pH7.5, 150mM NaCl, 0.5% Triton X-100). The proteins were eluted by heating in 20 µl laemelli buffer at 95^0C for 5min.

Cell counts

Cell counting of siRNA transfected cells in 12 well plates was performed 5d post transfection. Cells were trypsinized and changes in cell number assessed by cell counting in Countess II Lifetechnologies.

Immunoflourescence

LNCaP cells were seeded on to glass coverslips in a 12 well plate. After reaching 70-80% confluence, cells were transfected with scrambled or VPRBP siRNA. After 3 days, cells were fixed with 4% paraformaldehyde in BSA for 10 min followed by three washes in PBS for 5 min each. The fixed cells were then lysed in 0.1% TX100 in PBS for 10 min and blocked in blocking buffer (5% goat serum/1%BSA/0.1%TX100 in PBS) for 1h. The cells were then incubated in primary antibodies against VPRBP (1:80) and fibrillarin (1:100) for 2h at RT followed by Alexa flour 594 Goat anti mouse (Invitrogen, Cat # A11020) or Alexa flour 488 Goat Anti R (Invitrogen, Cat # A11070) secondary antibodies. Coverslips were mounted on to glass slides using Vectashield with DAPI.

Patients

Radical prostatectomy specimens were available from 3261 patients, consecutively treated at the Department of Urology, University Medical Center Hamburg-Eppendorf between 1992 and 2005 (Supplementary Table 6). Follow-up data were available for 2385 patients, ranging from 1 to 144 months (mean, 34 months). None of the patients received neo-adjuvant or adjuvant therapy. Additional (salvage) therapy was only initiated in case of a biochemical relapse (BCR). In all patients, prostate specific antigen (PSA) values were measured quarterly in the first year, followed by biannual measurements in the second and annual measurements after the third year following surgery. Recurrence was defined as a postoperative PSA of 0.1 ng/ml and rising. The first PSA value above or equal to 0.1 ng/ml was used to define the time of recurrence. Patients without evidence of tumor recurrence were censored at last follow-up. All prostatectomy specimens were analyzed according to a standard procedure. All prostates were completely paraffin-embedded, including whole-mount sections as previously described {Erbersdobler, 2002 #59}. One 0.6 mm tissue core was punched out from each case, and transferred in a tissue microarray (TMA) format as previously described (*24*). The 3261 cores were distributed among 7 TMA blocks each containing 129-522 tumor samples. Each TMA block also contained various control tissues including normal prostate tissue and other normal tissues.

The tissues and clinical data were utilized according to the Hamburger Krankenhaus Gesetz (§12 HmbKHG) and approved by our local Ethical Committee.

Immunohistochemistry

Freshly cut TMA sections were stained on one day in a single experiment. High-temperature pretreatment of slides was done in an autoclave in citrate buffer, pH 7.8 for 5 minutes. VPRBP immunostaining was performed using a monoclonal antibody (clone: EPR16012, Abcam; dilution: 1:450). The Envision system (DAKO) was used to visualize the immunostaining.

Only cytoplasmatic staining was evaluated. The staining intensity (0, 1+, 2+, 3+) and the fraction of positive tumor cells were recorded for each tissue spot. A final score was built from these two parameters according to the following scores: Negative scores had staining intensity of 0, weak scores had staining intensity of 1+ in ≤70% of tumor cells or staining intensity of 2+ in ≤30% of tumor cells; moderate scores had staining intensity of 1+ in >70% of tumor cells, staining intensity of 2+ in >30% and ≤70% of tumor cells or staining intensity of 3+ in ≤30% of tumor cells and strong scores had staining intensity of 2+ in >70% of tumor cells or staining intensity of 3+ in >30% of tumor cells.

Analysis of TCGA datasets

TCGA data was downloaded from cbioportal. Scatterplots showing normalized expression were plotted using R studio. ssGSEA was carried out using Genepattern. Single sample scores were calculated for h.all.v7.2 [Hallmarks] gene set in TCGA samples. Pearson correlation coefficient analysis was used to assess correlation.

Statistical analysis

Statistical analyses for studies in LNCaP and VCaP cells were done using either student's t-test or one way ANOVA with Tukey's posthoc analysis, as mentioned in the figure legends. For IHC, statistical calculations were performed using JMP 12® software (SAS Institute Inc., NC, USA). Contingency tables were calculated with the chi²-test. Survival curves were calculated by the Kaplan-Meier method and compared with the Log rank test.

References

1. Q. Feng, B. He, Androgen Receptor Signaling in the Development of Castration-Resistant Prostate Cancer. *Front Oncol* **9**, 858 (2019).
2. J. Munkley, Glycosylation is a global target for androgen control in prostate cancer cells. *Endocr Relat Cancer* **24**, R49-R64 (2017).
3. H. M. Itkonen *et al.*, O-GlcNAc transferase integrates metabolic pathways to regulate the stability of c-MYC in human prostate cancer cells. *Cancer Res* **73**, 5277-5287 (2013).

4. N. M. Akella, L. Ciraku, M. J. Reginato, Fueling the fire: emerging role of the hexosamine biosynthetic pathway in cancer. *BMC Biol* **17**, 52 (2019).
5. Y. Gu *et al.*, O-GlcNAcylation is increased in prostate cancer tissues and enhances malignancy of prostate cancer cells. *Mol Med Rep* **10**, 897-904 (2014).
6. M. R. Bond, J. A. Hanover, A little sugar goes a long way: the cell biology of O-GlcNAc. *J Cell Biol* **208**, 869-880 (2015).
7. Y. Fardini, V. Dehennaut, T. Lefebvre, T. Issad, O-GlcNAcylation: A New Cancer Hallmark? *Front Endocrinol (Lausanne)* **4**, 99 (2013).
8. T. Kamigaito *et al.*, Overexpression of O-GlcNAc by prostate cancer cells is significantly associated with poor prognosis of patients. *Prostate Cancer Prostatic Dis* **17**, 18-22 (2014).
9. Y. Zhu, X. Shan, S. A. Yuzwa, D. J. Vocadlo, The emerging link between O-GlcNAc and Alzheimer disease. *J Biol Chem* **289**, 34472-34481 (2014).
10. R. D. Semba, H. Huang, G. A. Lutty, J. E. Van Eyk, G. W. Hart, The role of O-GlcNAc signaling in the pathogenesis of diabetic retinopathy. *Proteomics Clin Appl* **8**, 218-231 (2014).
11. C. M. Ferrer, V. L. Sodi, M. J. Reginato, O-GlcNAcylation in Cancer Biology: Linking Metabolism and Signaling. *J Mol Biol* **428**, 3282-3294 (2016).
12. X. Yang, K. Qian, Protein O-GlcNAcylation: emerging mechanisms and functions. *Nat Rev Mol Cell Biol* **18**, 452-465 (2017).
13. W. H. Yang *et al.*, Modification of p53 with O-linked N-acetylglucosamine regulates p53 activity and stability. *Nat Cell Biol* **8**, 1074-1083 (2006).
14. H. M. Itkonen *et al.*, High OGT activity is essential for MYC-driven proliferation of prostate cancer cells. *Theranostics* **9**, 2183-2197 (2019).
15. C. E. Massie *et al.*, The androgen receptor fuels prostate cancer by regulating central metabolism and biosynthesis. *EMBO J* **30**, 2719-2733 (2011).
16. N. M. Schabla, K. Mondal, P. C. Swanson, DCAF1 (VprBP): emerging physiological roles for a unique dual-service E3 ubiquitin ligase substrate receptor. *J Mol Cell Biol* **11**, 725-735 (2019).
17. S. Zhang, Y. Feng, O. Narayan, L. J. Zhao, Cytoplasmic retention of HIV-1 regulatory protein Vpr by protein-protein interaction with a novel human cytoplasmic protein VprBP. *Gene* **263**, 131-140 (2001).
18. E. Le Rouzic *et al.*, HIV1 Vpr arrests the cell cycle by recruiting DCAF1/VprBP, a receptor of the Cul4-DDB1 ubiquitin ligase. *Cell Cycle* **6**, 182-188 (2007).
19. T. Nakagawa *et al.*, CRL4(VprBP) E3 ligase promotes monoubiquitylation and chromatin binding of TET dioxygenases. *Mol Cell* **57**, 247-260 (2015).
20. K. Kim *et al.*, VprBP has intrinsic kinase activity targeting histone H2A and represses gene transcription. *Mol Cell* **52**, 459-467 (2013).
21. C. M. McCall *et al.*, Human immunodeficiency virus type 1 Vpr-binding protein VprBP, a WD40 protein associated with the DDB1-CUL4 E3 ubiquitin ligase, is essential for DNA replication and embryonic development. *Mol Cell Biol* **28**, 5621-5633 (2008).
22. B. Langmead, S. L. Salzberg, Fast gapped-read alignment with Bowtie 2. *Nat Methods* **9**, 357-359 (2012).
23. J. Feng, T. Liu, Y. Zhang, Using MACS to identify peaks from ChIP-Seq data. *Curr Protoc Bioinformatics* **Chapter 2**, Unit 2 14 (2011).
24. L. Bubendorf *et al.*, Survey of gene amplifications during prostate cancer progression by high-throughout fluorescence in situ hybridization on tissue microarrays. *Cancer Res* **59**, 803-806 (1999).
25. Z. Guo *et al.*, DCAF1 controls T-cell function via p53-dependent and -independent mechanisms. *Nat Commun* **7**, 10307 (2016).
26. P. W. Lo *et al.*, O-GlcNAcylation regulates the stability and enzymatic activity of the histone methyltransferase EZH2. *Proc Natl Acad Sci U S A* **115**, 7302-7307 (2018).
27. S. E. S. Martin *et al.*, Structure-Based Evolution of Low Nanomolar O-GlcNAc Transferase Inhibitors. *J Am Chem Soc* **140**, 13542-13545 (2018).

28. A. Karimian, Y. Ahmadi, B. Yousefi, Multiple functions of p21 in cell cycle, apoptosis and transcriptional regulation after DNA damage. *DNA Repair (Amst)* **42**, 63-71 (2016).
29. Y. Barak, T. Juven, R. Haffner, M. Oren, mdm2 expression is induced by wild type p53 activity. *EMBO J* **12**, 461-468 (1993).
30. A. M. Barsotti, C. Prives, Pro-proliferative FoxM1 is a target of p53-mediated repression. *Oncogene* **28**, 4295-4305 (2009).
31. Y. Gu, J. Rosenblatt, D. O. Morgan, Cell cycle regulation of CDK2 activity by phosphorylation of Thr160 and Tyr15. *EMBO J* **11**, 3995-4005 (1992).
32. A. Lindqvist, W. van Zon, C. Karlsson Rosenthal, R. M. Wolthuis, Cyclin B1-Cdk1 activation continues after centrosome separation to control mitotic progression. *PLoS Biol* **5**, e123 (2007).
33. L. Gheghiani, D. Loew, B. Lombard, J. Mansfeld, O. Gavet, PLK1 Activation in Late G2 Sets Up Commitment to Mitosis. *Cell Rep* **19**, 2060-2073 (2017).
34. A. Van Hooser, D. W. Goodrich, C. D. Allis, B. R. Brinkley, M. A. Mancini, Histone H3 phosphorylation is required for the initiation, but not maintenance, of mammalian chromosome condensation. *J Cell Sci* **111 (Pt 23)**, 3497-3506 (1998).
35. N. Berndt, M. Dohadwala, C. W. Liu, Constitutively active protein phosphatase 1alpha causes Rb-dependent G1 arrest in human cancer cells. *Curr Biol* **7**, 375-386 (1997).
36. Z. Andrysik *et al.*, Identification of a core TP53 transcriptional program with highly distributed tumor suppressive activity. *Genome Res* **27**, 1645-1657 (2017).
37. M. A. Sammons, J. Zhu, A. M. Drake, S. L. Berger, TP53 engagement with the genome occurs in distinct local chromatin environments via pioneer factor activity. *Genome Res* **25**, 179-188 (2015).
38. Q. Zeidan, Z. Wang, A. De Maio, G. W. Hart, O-GlcNAc cycling enzymes associate with the translational machinery and modify core ribosomal proteins. *Mol Biol Cell* **21**, 1922-1936 (2010).
39. L. Badertscher *et al.*, Genome-wide RNAi Screening Identifies Protein Modules Required for 40S Subunit Synthesis in Human Cells. *Cell Rep* **13**, 2879-2891 (2015).
40. A. James, Y. Wang, H. Raje, R. Rosby, P. DiMario, Nucleolar stress with and without p53. *Nucleus* **5**, 402-426 (2014).
41. J. P. Belzile, L. G. Abrahamyan, F. C. Gerard, N. Rougeau, E. A. Cohen, Formation of mobile chromatin-associated nuclear foci containing HIV-1 Vpr and VPRBP is critical for the induction of G2 cell cycle arrest. *PLoS Pathog* **6**, e1001080 (2010).
42. C. Stark *et al.*, BioGRID: a general repository for interaction datasets. *Nucleic Acids Res* **34**, D535-539 (2006).
43. P. J. Thul *et al.*, A subcellular map of the human proteome. *Science* **356**, (2017).
44. K. Yang, J. Yang, J. Yi, Nucleolar Stress: hallmarks, sensing mechanism and diseases. *Cell Stress* **2**, 125-140 (2018).
45. Y. Li, Y. Hu, L. Che, J. Jia, M. Chen, Nucleolar localization of Small G protein RhoA is associated with active RNA synthesis in human carcinoma HEp-2 cells. *Oncol Lett* **11**, 3605-3610 (2016).
46. G. M. Lingaraju *et al.*, Crystal structure of the human COP9 signalosome. *Nature* **512**, 161-165 (2014).
47. D. Bech-Otschir *et al.*, COP9 signalosome-specific phosphorylation targets p53 to degradation by the ubiquitin system. *EMBO J* **20**, 1630-1639 (2001).
48. T. Y. Chou, G. W. Hart, C. V. Dang, c-Myc is glycosylated at threonine 58, a known phosphorylation site and a mutational hot spot in lymphomas. *J Biol Chem* **270**, 18961-18965 (1995).
49. D. Hawksworth *et al.*, Overexpression of C-MYC oncogene in prostate cancer predicts biochemical recurrence. *Prostate Cancer Prostatic Dis* **13**, 311-315 (2010).
50. K. Hrecka *et al.*, Lentiviral Vpr usurps Cul4-DDB1[VprBP] E3 ubiquitin ligase to modulate cell cycle. *Proc Natl Acad Sci U S A* **104**, 11778-11783 (2007).

51. S. S. Gabriel, A. Kallies, Glucose- and glutamine-fueled stabilization of C-Myc is required for T-cell proliferation and malignant transformation. *Cell Death Discov* **2**, 16047 (2016).
52. M. Swamy *et al.*, Glucose and glutamine fuel protein O-GlcNAcylation to control T cell self-renewal and malignancy. *Nat Immunol* **17**, 712-720 (2016).
53. K. Kim *et al.*, Vpr-binding protein antagonizes p53-mediated transcription via direct interaction with H3 tail. *Mol Cell Biol* **32**, 783-796 (2012).
54. A. Balasubramani, A. Rao, O-GlcNAcylation and 5-methylcytosine oxidation: an unexpected association between OGT and TETs. *Mol Cell* **49**, 618-619 (2013).
55. S. J. Barfeld *et al.*, Myc-dependent purine biosynthesis affects nucleolar stress and therapy response in prostate cancer. *Oncotarget* **6**, 12587-12602 (2015).
56. H. W. Sollinger, Mycophenolate mofetil. *Kidney Int Suppl* **52**, S14-17 (1995).
57. S. Cavadini *et al.*, Cullin-RING ubiquitin E3 ligase regulation by the COP9 signalosome. *Nature* **531**, 598-603 (2016).
58. A. M. Bode, Z. Dong, Post-translational modification of p53 in tumorigenesis. *Nat Rev Cancer* **4**, 793-805 (2004).
59. M. H. Lee, R. Zhao, L. Phan, S. C. Yeung, Roles of COP9 signalosome in cancer. *Cell Cycle* **10**, 3057-3066 (2011).
60. T. A. Soucy *et al.*, An inhibitor of NEDD8-activating enzyme as a new approach to treat cancer. *Nature* **458**, 732-736 (2009).
61. A. Schlierf *et al.*, Targeted inhibition of the COP9 signalosome for treatment of cancer. *Nat Commun* **7**, 13166 (2016).
62. J. J. Shah *et al.*, Phase I Study of the Novel Investigational NEDD8-Activating Enzyme Inhibitor Pevonedistat (MLN4924) in Patients with Relapsed/Refractory Multiple Myeloma or Lymphoma. *Clin Cancer Res* **22**, 34-43 (2016).
63. J. Sarantopoulos *et al.*, Phase I Study of the Investigational NEDD8-Activating Enzyme Inhibitor Pevonedistat (TAK-924/MLN4924) in Patients with Advanced Solid Tumors. *Clin Cancer Res* **22**, 847-857 (2016).
64. P. Chen *et al.*, Neddylation Inhibition Activates the Extrinsic Apoptosis Pathway through ATF4-CHOP-DR5 Axis in Human Esophageal Cancer Cells. *Clin Cancer Res* **22**, 4145-4157 (2016).
65. M. El-Mesery *et al.*, The NEDD8-activating enzyme inhibitor MLN4924 sensitizes a TNFR1(+) subgroup of multiple myeloma cells for TNF-induced cell death. *Cell Death Dis* **10**, 611 (2019).

Acknowledgment

This research was supported by the Norwegian Research Council (230559). IGM is also supported by the Prostate Cancer UK/ Movember Centre of Excellence (CEO13_2–004) and the John Black Charitable Foundation. Authors would like to acknowledge Genomic Core Technology Units, Queens University Belfast for the assistance with ChIP-seq studies.

Author contributions

NP designed and performed the experiments, prepared samples for sequencing, analyzed the data and wrote the manuscript. AP, GS and Sarah Minner performed IHC and evaluated

expression in prostate tumours. NF performed analysis on TCGA datasets. GG generated p53 knockout LNCaP cells under the supervision of SMcD. SMcD reviewed and edited the manuscript. MF performed the fragment analysis for ChIP-seq samples and conducted the Illumina NextSeq™ 500 sequencing run. Sarah Maguire generated the fastq files, bam files and bed files. IGM supervised the study, reviewed and edited the manuscript.

Declaration of Interests

The authors declare no competing interests.

Figure legends

Figure 1. Identification of VPRBP as an AR and O-GlcNAc co-regulated target from ChIP-seq analysis of published datasets. (A) Venn diagrams showing the distribution of peaks in relation to genes in AR and OGlcNAc consensus ChIP-seq, generated using CEAS (Cis-regulatory element annotation system) tool in galaxy cistrome. (B) ChIP-seq enrichment of AR and O-GlcNAc at VPRBP promoter region using UCSC genome browser. (C) Percentage recovery of CAMKK2 and VPRBP with AR ChIP; and PPAT/PAICS and VPRBP with O-GlcNAc ChIP in vehicle (0.01% ethanol) and 1nM R1881 4h and 24h treated LNCaP cells. (D) mRNA expression of VPRBP, CAMKK2 and UAP1 in LNCaP treated with vehicle or 1nM R1881 for 24 h was detected by quantitative reverse transcription-PCR (qRT-PCR). Results are normalized to RPLPO as housekeeping control. (E) Time dependency of VPRBP expression following exposure to 1nM R1881 for different time points. LNCaP cells were androgen deprived for 3 days prior to stimulation with vehicle or 1 nM R1881. Different time points were calculated from the time of cell lysis and all samples processed at the same time for immunoblot analysis. Data are mean ± SD from at least three independent experiments. p values by two-sided Student's t test. ** =$p < 0.01$; *** = $p < 0.001$.

Figure 2. OGT is required for VPRBP stability. (A) LNCaP cells were transiently transfected with OGT siRNA and cells were harvested 5d post transfection to detect mRNA expression of VPRBP, OGT and OGA by qRT-PCR and (B) protein expression by immunoblot analysis under basal conditions. (C) For detection of protein expression under androgen stimulated conditions, LNCaP cells were transfected with OGT siRNAs or scrambled siRNA (scr si) followed by androgen deprivation for 72 h prior to 1nM R1881 stimulation for 24h. (D) The O-GlcNAcylation of immunoprecipitated (IP) VPRBP from LNCaP cells was detected by immunoblotting (IB) with RL2 antibody. (E) The effect of OGT inhibitors 40 μM OSMI2 and 10 μM OSMI3 on VPRBP protein levels following 24h treatment was detected by immnuoblot analysis. Results are expressed as means ± SD. *** = $p < 0.001$ by Student's t test.

Figure 3. VPRBP knockdown leads to reduced cell proliferation and p53 stabilization. (A) LNCaP cells were transfected with VPRBP siRNA and cells were harvested 3d post transfection to detect mRNA expression of VPRBP, OGT, p53 and p21. (B) Effect of VPRBP knockdown on LNCaP cell proliferation was assessed by cell counting 5d post transfection; the cells were grown in the presence (CM) and absence of androgens (ADM). (C) Effect of VPRBP knockdown on LNCaP p53, markers of cell cycle and other proteins of interest was assessed by immunoblot analysis of cell lysate prepared 3d post transfection. (D) Effect of VPRBP knockdown on cell proliferation was assessed by cell counting 5d post transfection in VCaP cells grown in the presence (CM) and absence of androgens (ADM). (E) Effect of VPRBP knockdown on VCaP proteins of interest was assessed by immunoblot analysis. Results are expressed as means ± SD. * =$p < 0.05$, ** =$p < 0.01$; *** = $p < 0.00$. Statistical analyses were performed by Student's t test for qPCR and one-way ANOVA followed by Tukey's posthoc analysis for cell proliferation.

Figure 4. VPRBP knockdown increases p53 chromatin recruitment and induces nucleolar stress. (A) Bar graph showing percentage recovery of p21 and negative primer (CCND1)

following p53 ChIP in different transfection conditions. (B) Table showing the number of peaks obtained under different conditions. (C) Venn diagram showing the overlap of our nutlin-3a p53 ChIP-seq in LNCaP cells with previously reported nutlin-3a p53 ChIP-seq in MCF7 cells. (D) Venn diagram showing the overlap of nutlin-3a p53 ChIP-seq in LNCaP with VPRBPsi p53 ChIP-seq consensus sites. (E) Venn diagram showing the overlap of VPRBPsi p53 ChIP-seq consensus sites with previously reported nutlin-3a p53 ChIP-seq in MCF7 cells. (F) Venn diagram showing the overlap of VPRBP interactome with nucleolar proteome. (G) Representative immunofluorescence images showing VPRBP and fibrillarin staining in scrambled and VPRBP siRNA transfected LNCaPs 3d post transfection (scale bar= 10μm).

Figure 5. VPRBP stability is regulated by COP9 signalosome. COPS3 mRNA expression in LNCaP cells treated with vehicle or 1nM R1881 for 24 h was detected by qRT-PCR (A) and protein expression by immunoblot analysis (B and C). (D) LNCaP cells were transfected with COPS3 siRNA and cells were harvested 3d post transfection to detect mRNA expression of VPRBP and COSP3. (E) Effect of COPS3 knockdown on VPRBP, p53 and other proteins of interest was assessed by immunoblot analysis. (F) Effect of COPS3 knockdown on cell proliferation was assessed by cell counting 5d post transfection in LNCaPs grown in complete media. (G) Effect of neddylation activation enzyme inhibitor, MLN4924 on LNCaP proliferation was assessed by cell counting. (H) For combination studies, cells were treated simultaneously with single dose of both inhibitors. * =$p < 0.05$, ** =$p < 0.01$; *** = $p < 0.001$; statistical analyses for cell proliferation studies was done by one way ANOVA and Tukey's posthoc analysis; for others student's t test was conducted.

Figure 6. VPRBP protein expression correlates with AR overexpression, OGT overexpression and poor prognosis. Bar graphs showing positive correlation of VPRBP expression with AR (A) and OGT expression (B) by IHC on TMA sections.. (C) PSA recurrence free survival curves with combination of markers, AR and VPRBP, and (D)

combination of OGT and VPRBP. (E) Scatter plot comparing AR mRNA expression to VRPBP mRNA expression in TCGA PanCancer Atlas prostate dataset. P-value = <0.001 (F) Scatter plot comparing GSEA Hallmark "P53 Pathway" to VRPBP mRNA expression in TCGA PanCancer Atlas prostate dataset. P-value = 0.0001, Correlation Coefficient = -0.172.

Supplementary figures

Supplementary Figure S1. (A) Bar graphs showing relative enrichments in CAMKK2 and VPRBP with AR ChIP-qPCR in vehicle vs R1881 (24h) treated LNCaP cells; and relative enrichments in PPAT/PAICS and VPRBP with O-GlcNAc ChIP. (B) Graphs showing quantitation of western bands of Figure 1E done using image J software and normalized to β-actin. (C) qRT-PCR analysis of VPRBP, CAMKK2 and UAP1 expression in LNCaP cells treated with vehicle (0.01% ethanol) or 1nM DHT for 24h following androgen deprivation for 72h. (D) Western blot analysis of LNCaP cells treated with vehicle or DHT (1nM and 10nM) for 24 h. Results are expressed as means ± SD. * =$p < 0.05$, ** =$p < 0.01$; *** = $p < 0.001$ by Student's t test.

Supplementary Figure S2. VPRBP and p53 exhibit reciprocal relation. (A) Western image showing time dependent reduction in p53 expression following exposure to 1nM R1881 for different time points. (B) qRT-PCR analysis of p53 expression in LNCaP cells treated with vehicle or 1nM R1881 for 24h with RPLPO as internal control. (C) Bar graphs showing relative enrichments in p21 with p53 ChIP-qPCR in vehicle and R1881 24h treated LNCaP cells. (D) Bar graphs showing percentage recovery of p21, VPRBP and negative primers with p53 ChIP-qPCR in vehicle (DMSO) and Nutlin-3a 24h treated LNCaP. (E) ChIP-seq enrichment profile of nutlin-3a p53 ChIP-seq at CDKN1A (p21) promoter region (top) and absence of enrichment at VPRBP promoter region (bottom), using UCSC genome browser. (F) Protein expression of

VPRBP, p53 and p21 by immunoblot analysis following vehicle and Nutlin-3a treatment for 24h; and wild type versus p53 knockout LNCaP cells, and (G) mRNA expression by qRT-PCR. Results are expressed as means ± SD. *** = $p < 0.001$ by Student's t test.

Supplementary Figure S3. OGT is required for VPRBP stability. (A) Graphs showing quantitation of western bands (Figure 2B) from OGT siRNA transfected cells vs scrambled control using image J software and normalized to β-actin. (B) Graphs showing quantitation of western bands (Figure 2E) from OSMI2/OSMI3 treatments and normalized to β-actin. (C) qRT-PCR analysis VPRBP and OGT expression in LNCaP cells treated with vehicle or 40 μM OSMI2 or 10 μM OSMI3 for 24h with RPLPO as internal control. Results are expressed as means ± SD. * =$p < 0.05$, ** =$p < 0.01$; *** = $p < 0.001$ by Student's t test.

Supplementary Figure S4. (A) Effect of VPRBP kinase activity inhibitor, B32B3 on LNCaP cell proliferation was assessed by cell counting 4d post treatment in the presence and absence of OSMI2 and OSMI3. (B) Effect of B32B3 on Histone H2A threonine 120 phosphorylation by immunoblot analysis. (C) Graphs showing quantitation of western bands (Figure 3C) from VPRBP siRNA transfected cells *vs* scrambled control using image J software and normalized to β-actin. (D) Effect of OGT knockdown on LNCaP cell proliferation was assessed by cell counting 5d post transfection. Results are expressed as means ± SD. * =$p < 0.05$, ** =$p < 0.01$; *** = $p < 0.001$ by Student's t test.

Supplementary Figure S5. (A) Screenshot of the top ChIP-seq datasets which show overlap with our LNCaP nutlin-3a p53 ChIP-seq data in ChIP Atlas. (B) Venn diagram showing the overlap of our nutlin-3a p53 ChIP-seq in LNCaP with previously reported nutlin-3a p53 ChIP-seq in HCT116, Bone/SJSA and IMR90 fetal lung fibroblasts. (C) Venn diagram showing the overlap of VPRBP si1 and VPRBP si2 p53 ChIP-seq peaks; overlap of OGT si1 and OGT si2 p53 ChIP seq peaks; and overlap of scr, VPRBPsi and OGTsi ChIP-seq peaks. (D) CEAS

analysis of VPRBP si p53 ChIP-seq in LNCaP and nutlin-3a p53 ChIP-seq in MCF7. (E) Table showing the top over-represented motifs obtained from motif enrichment analysis of VPRBP si p53 ChIP-seq using P-scan ChIP.

Supplementary Figure S6. (A) Effect of VPRBP knockdown on fibrillarin, RPS8 and RPL5 was assessed by immunoblot analysis and (B) graphs showing quantitation of the western bands. (C) Survival curve showing inverse relation between VPRBP expression and PSA recurrence free survival (D) IHC representative images showing negative, weak, moderate and strong staining of VPRBP. Results are expressed as means ± SD. * =$p < 0.05$ by Student's t test.

Figure 1

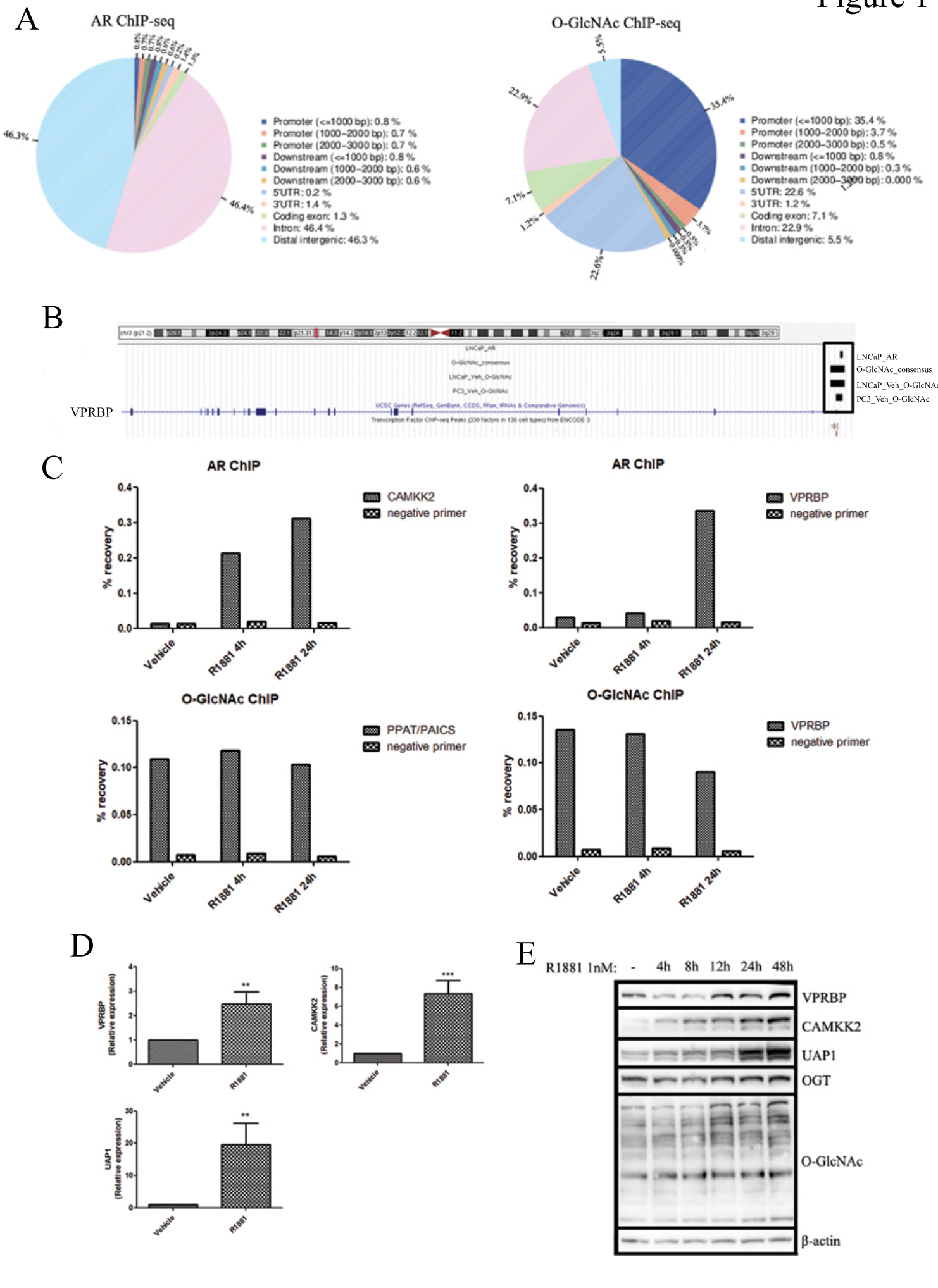
A
AR ChIP-seq
46.3%
46.4%
Promoter (<=1000 bp): 0.8 %
Promoter (1000-2000 bp): 0.7 %
Promoter (2000-3000 bp): 0.7 %
Downstream (<=1000 bp): 0.8 %
Downstream (1000-2000 bp): 0.6 %
Downstream (2000-3000 bp): 0.6 %
5'UTR: 0.2 %
3'UTR: 1.4 %
Coding exon: 1.3 %
Intron: 46.4 %
Distal intergenic: 46.3 %
O-GlcNAc ChIP-seq
35.4%
22.9%
7.1%
1.2%
22.6%
5.5%
Promoter (<=1000 bp): 35.4 %
Promoter (1000-2000 bp): 3.7 %
Promoter (2000-3000 bp): 0.5 %
Downstream (<=1000 bp): 0.8 %
Downstream (1000-2000 bp): 0.3 %
Downstream (2000-3000 bp): 0.000 %
5'UTR: 22.6 %
3'UTR: 1.2 %
Coding exon: 7.1 %
Intron: 22.9 %
Distal intergenic: 5.5 %
B
LNCaP_AR
O-GlcNAc_consensus
LNCaP_Veh_O-GlcNAc
PC3_Veh_O-GlcNAc
VPRBP
C
AR ChIP
% recovery
CAMKK2
negative primer
Vehicle
R1881 4h
R1881 24h
AR ChIP
VPRBP
negative primer
O-GlcNAc ChIP
PPAT/PAICS
negative primer
O-GlcNAc ChIP
VPRBP
negative primer
D
VPRBP (Relative expression)
CAMKK2 (Relative expression)
UAP1 (Relative expression)
Vehicle
R1881
E
R1881 1nM: - 4h 8h 12h 24h 48h
VPRBP
CAMKK2
UAP1
OGT
O-GlcNAc
β-actin

Figure 2

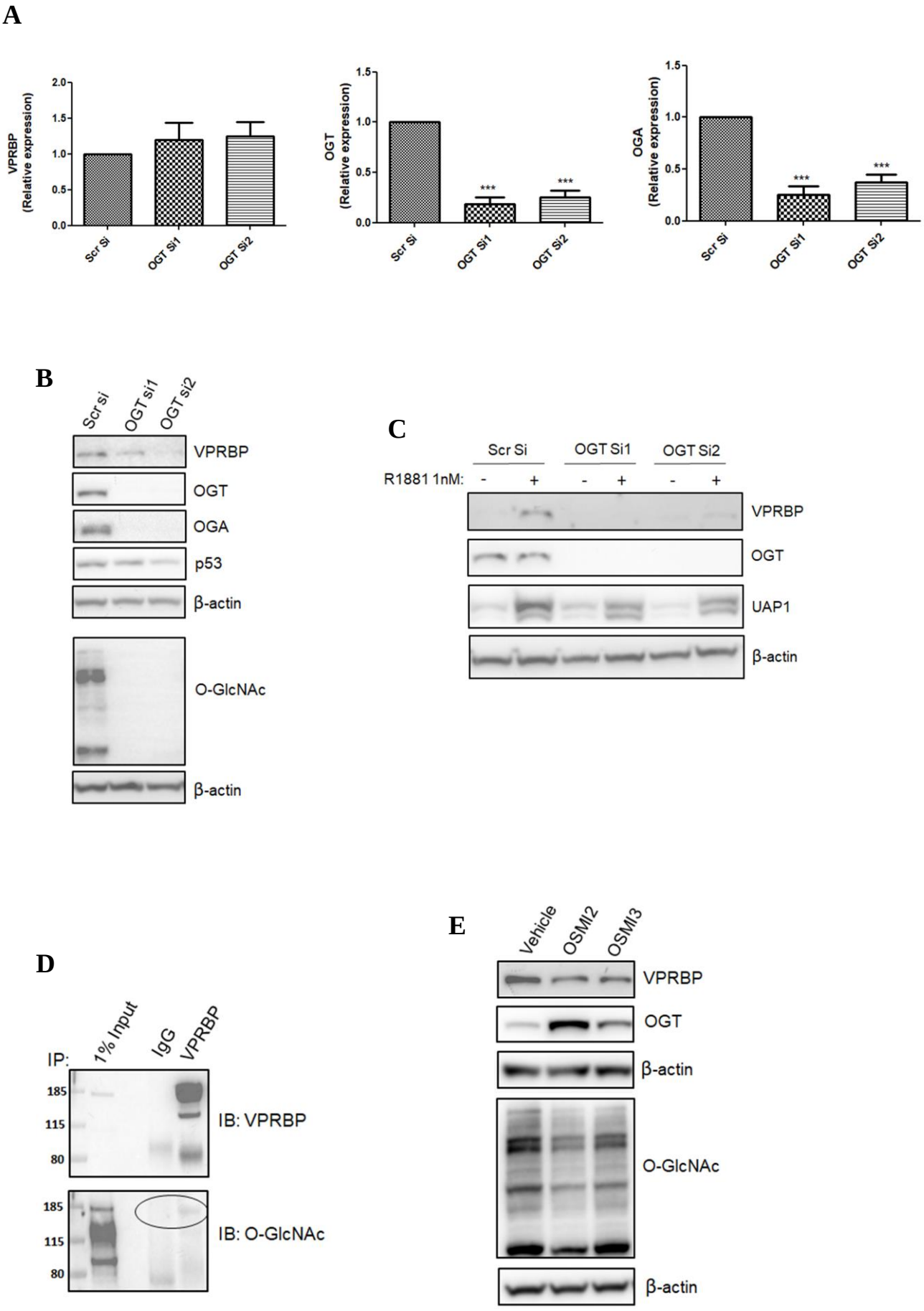

Figure 3

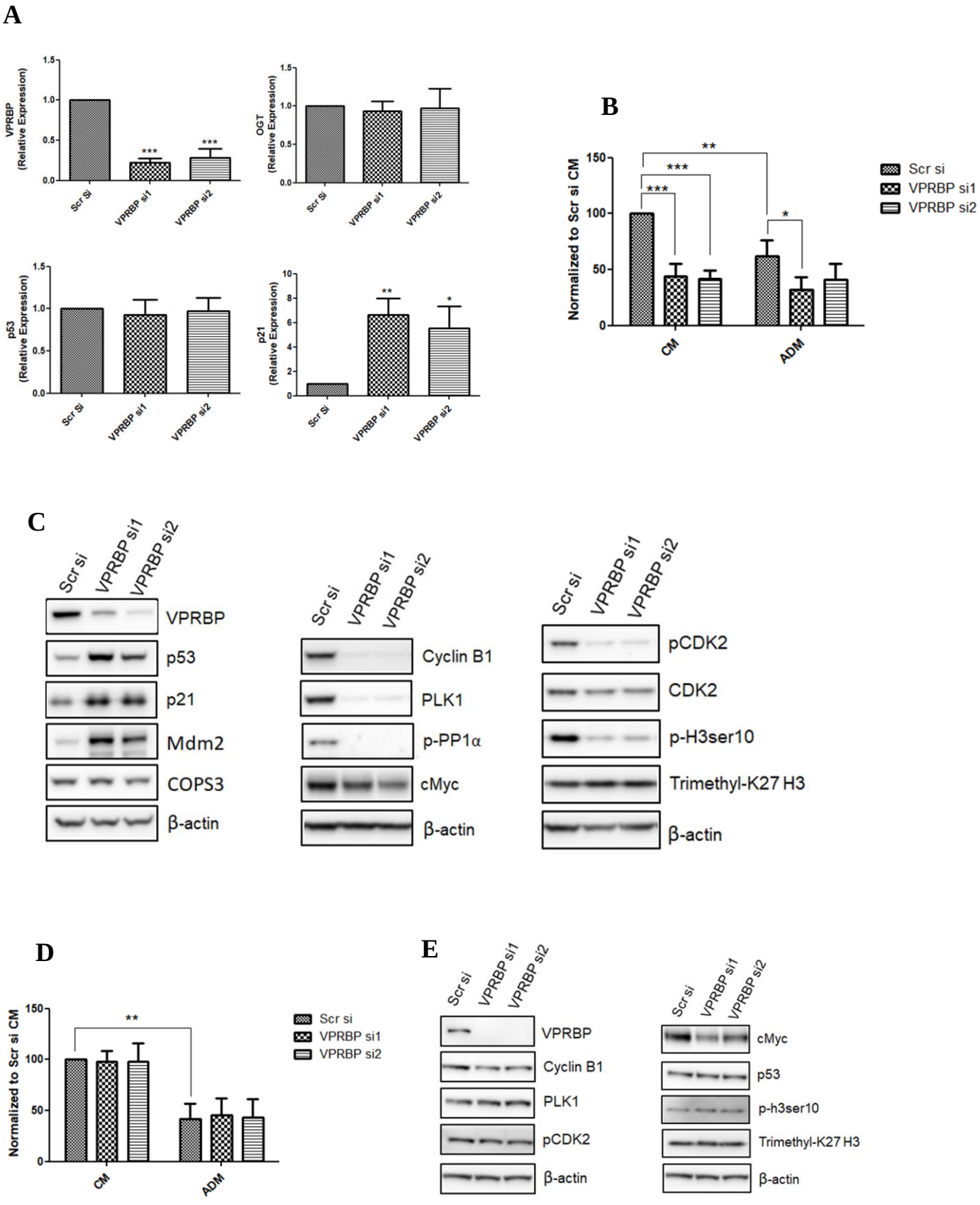

Figure 4

A

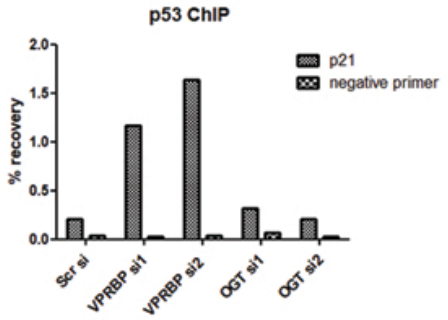

B

ChIP conditions	Number of peaks
LNCaP_VPRBP_Si1_p53	2326
LNCaP_VPRBP_Si2_p53	1639
LNCaP_Nutlin_3A_p53	582
LNCaP_OGT_Si1_p53	412
LNCaP_OGT_Si1_p53	423
LNCaP_Scr_Si_p53	425

C

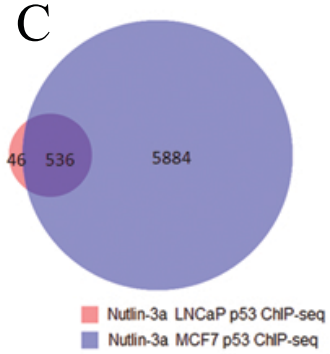

D

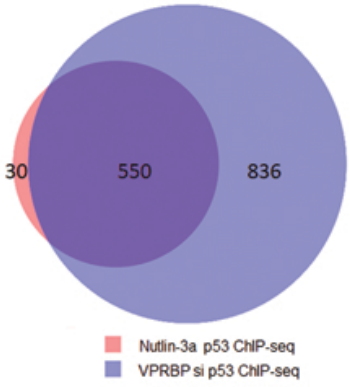

E

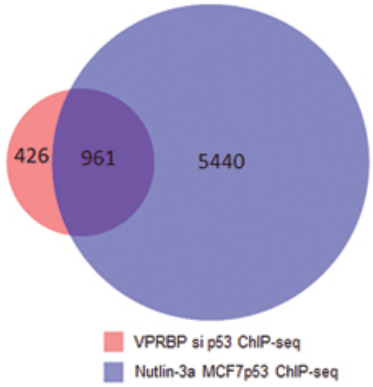

F

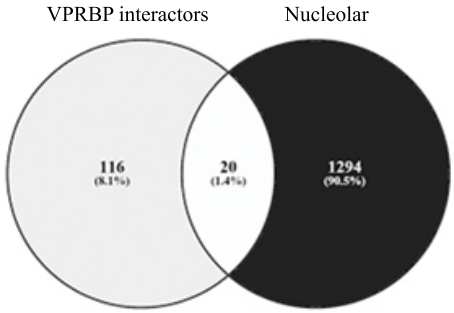

G

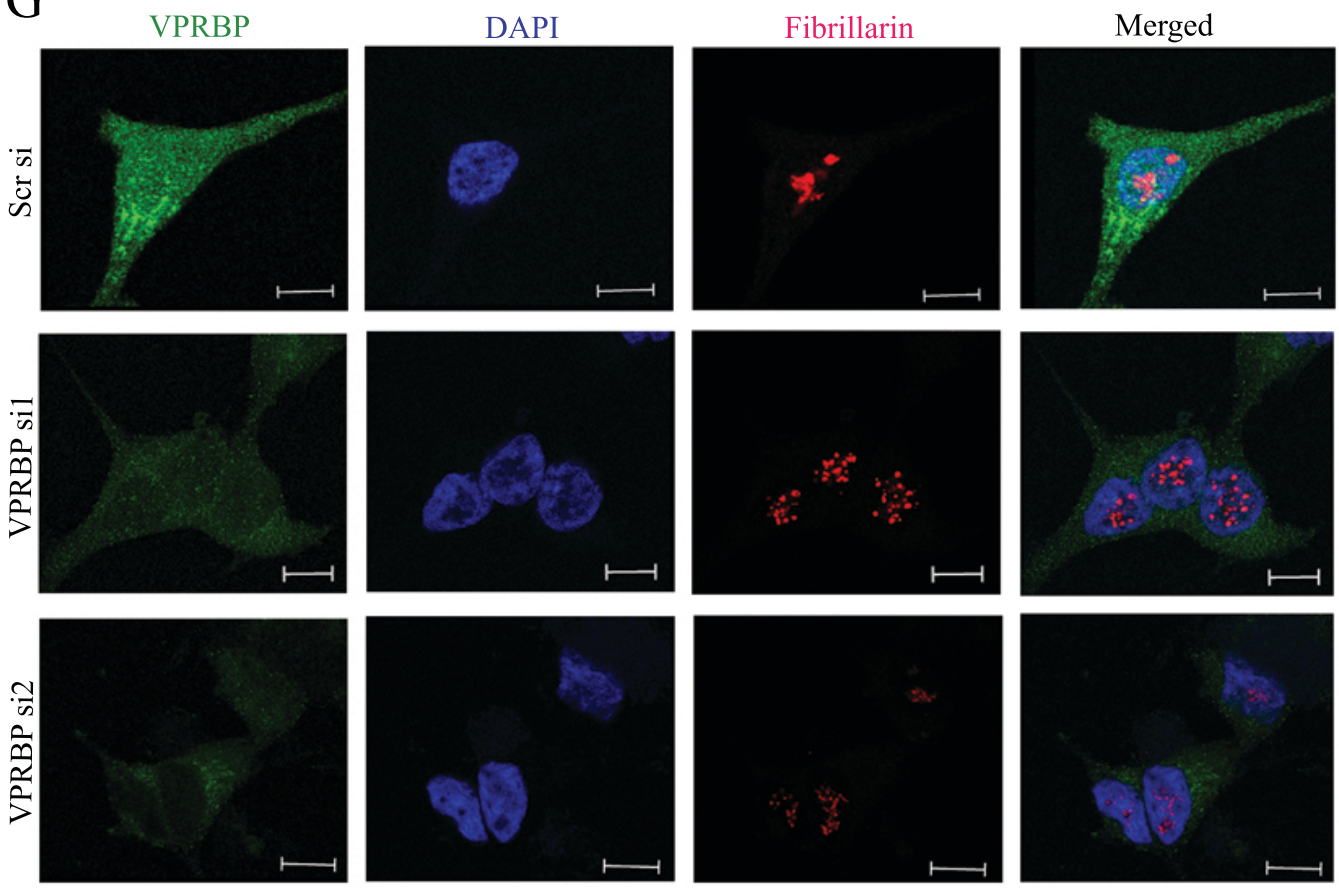

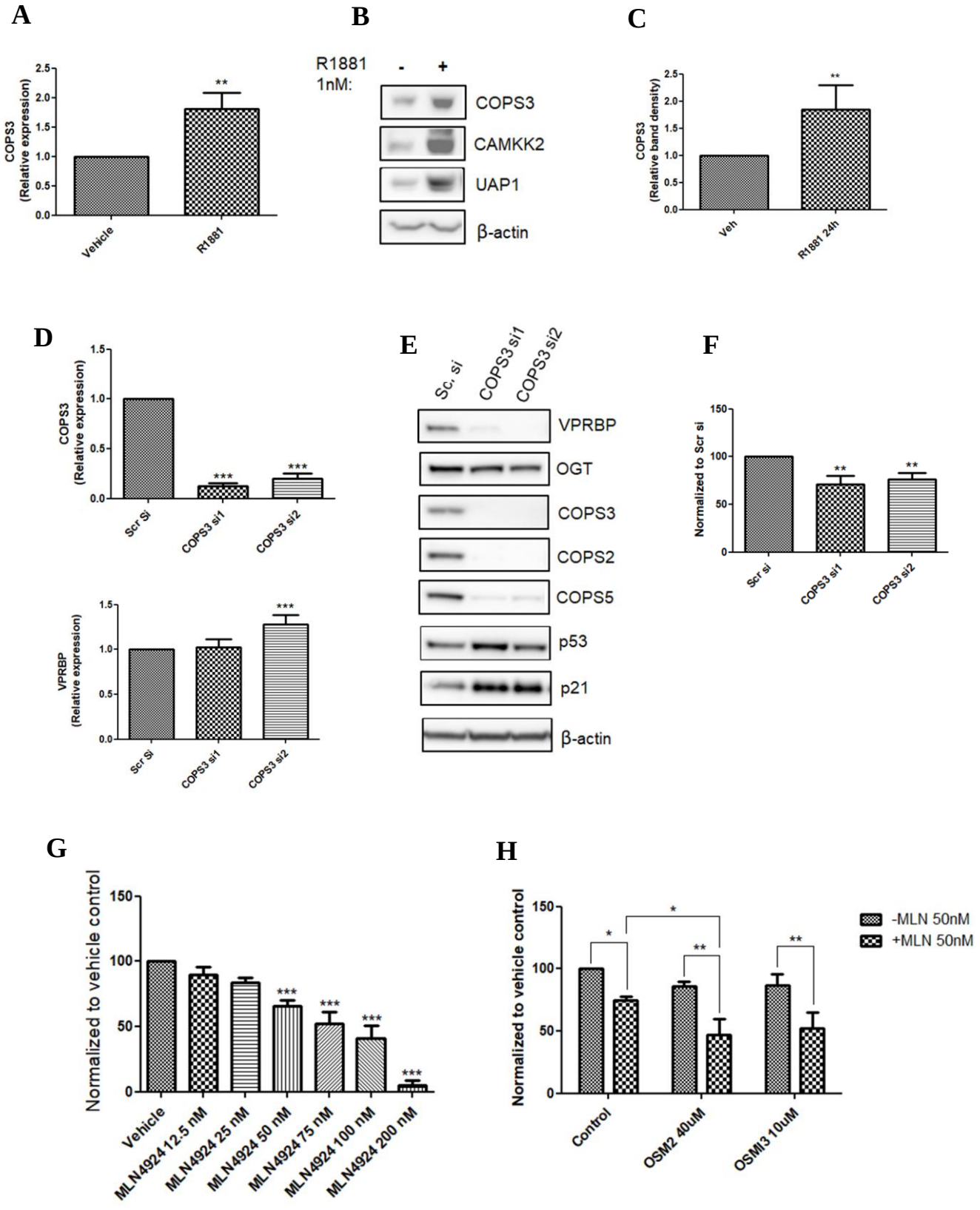

A

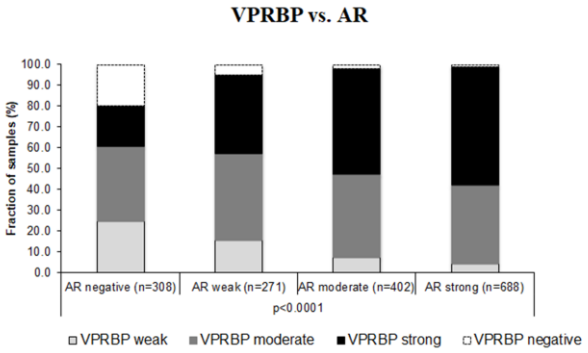

B

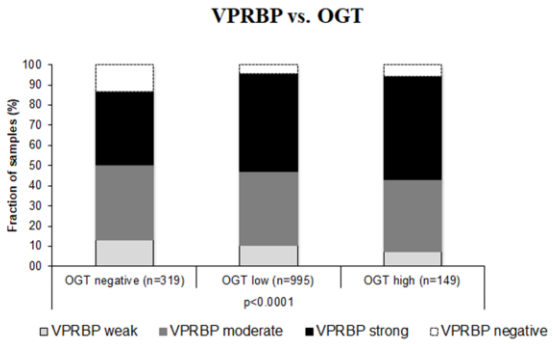

C

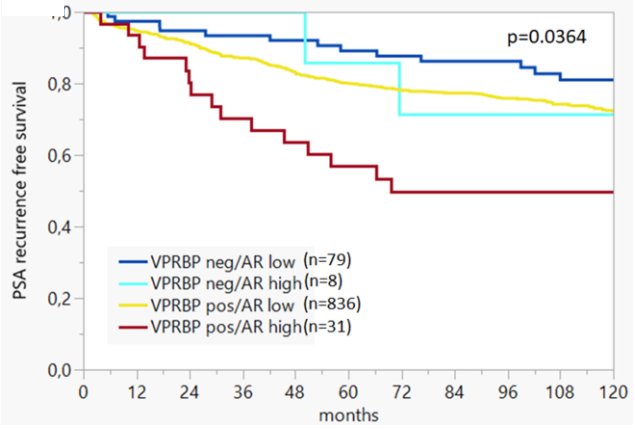

D

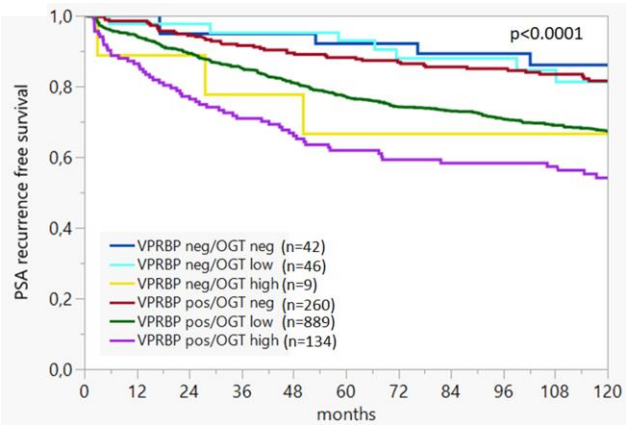

E

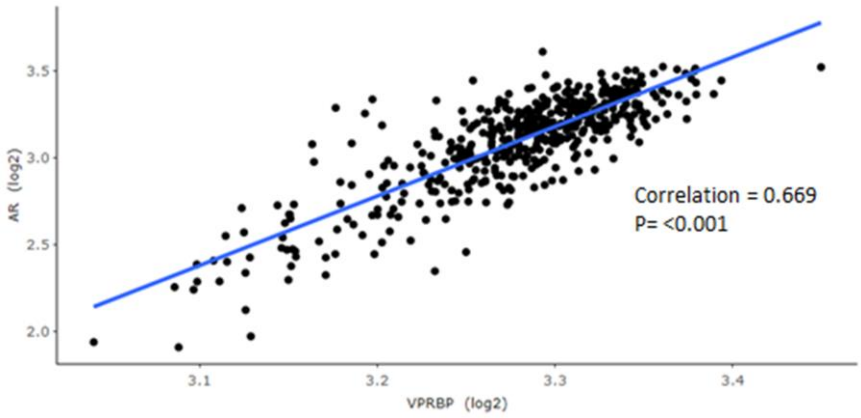

F